*Energies* **2012**, *5*, 4251-4267; doi:10.3390/en5114251

OPEN ACCESS

*energies*

**ISSN 1996-1073**

www.mdpi.com/journal/energies

*Article*

# Experimental Characterization of the Poisoning Effects of Methanol-Based Reformate Impurities on a PBI-Based High Temperature PEM Fuel Cell

**Samuel Simon Araya *, Søren Juhl Andreasen and Søren Knudsen Kær**

Department of Energy Technology, Aalborg University, Pontoppidanstræde 101, Aalborg East 9220, Denmark; E-Mails: sja@et.aau.dk (S.J.A.); skk@et.aau.dk (S.K.K.)

* Author to whom correspondence should be addressed; E-Mail: ssa@et.aau.dk; Tel.: +45-2137-1172; Fax: +45-9815-1411.

*Received: 3 August 2012; in revised form: 9 October 2012 / Accepted: 18 October 2012 / Published: 24 October 2012*

---

**Abstract:** In this work the effects of reformate gas impurities on a $H_3PO_4$-doped polybenzimidazole (PBI) membrane-based high temperature proton exchange membrane fuel cell (HT-PEMFC) are studied. A unit cell assembly with a BASF Celtec®-P2100 high temperature membrane electrode assembly (MEA) of 45 $cm^2$ active surface area is investigated by means of impedance spectroscopy. The concentrations in the anode feed gas of all impurities, unconverted methanol-water vapor mixture, CO and $CO_2$ were varied along with current density according to a multilevel factorial design of experiments. Results show that all the impurities degrade the performance, with CO being the most degrading agent and $CO_2$ the least. The factorial analysis shows that there is interdependence among the effects of the different factors considered. This interdependence suggests, for example, that tolerances to concentrations of CO above 2% may be compromised by the presence in the anode feed of $CO_2$. Methanol has a poisoning effect on the fuel cell at all the tested feed ratios, and the performance drop is found to be proportional to the amount of methanol in feed gas. The effects are more pronounced when other impurities are also present in the feed gas, especially at higher methanol concentrations.

**Keywords:** high temperature PEM fuel cell; methanol; $CO_2$; CO; Electrochemical Impedance Spectroscopy (EIS)

---

## 1. Introduction

For fuel cell applications, methanol allows more practical energy storage compared to either compressed or liquid hydrogen. It is liquid at room temperature, and therefore, it can use existing gasoline infrastructure with only few modifications [1,2]. This makes its storage and distribution much less complex than the required hydrogen infrastructure. Unlike natural gas, gasoline and other fossil fuel sources of hydrogen, it can be $CO_2$ neutral if prepared from renewable from various biomass sources such as wood, forest waste, peat, municipal solid wastes, sewage and even chemical recycling of $CO_2$ in the atmosphere [3,4].

Moreover, owing to its lower-energy chemical bonds, *i.e.*, the absence of C-C bonds, methanol has the advantage of requiring lower reforming temperatures of about 250 to 300 °C compared to other hydrocarbon fuels, where the required temperature is 800 to 900 °C [5]. The methanol reforming temperature can further be reduced to around 200 °C, comparable to the operating temperatures of an HT-PEMFC, with good conversion efficiencies and low CO contents, but lower hydrogen yield [6]. This is desirable as it opens new opportunities, making methanol increasingly proposed for on-board reforming to hydrogen and carbon dioxide for indirect methanol fuel cells, including HT-PEMFC [6–8].

In spite of all these compelling advantages that methanol has over other sources of hydrogen for use in fuel cells, the outcome of its steam reforming process is not clean hydrogen. It is hydrogen-rich mixture of gases and vapors, known as reformate gas, that contains a number of impurities with potential poisoning effects on a fuel cell. These impurities are CO, $CO_2$ and unconverted methanol and water vapor mixture.

Recently, research has been focusing on characterizing the poisoning effects of CO and $CO_2$ in both low and high temperature PEM fuel cells, in order to understand the mechanisms by which they affect the performance of fuel cells [9–13]. It is widely recognized that CO is the main catalyst poison amongst the impurities in a reformate gas. It adsorbs at the surface of platinum electro-catalysts and occupies active sites that could otherwise be used for catalysis [11]. Tolerance of PEM fuel cells to the poisoning effect of CO increases with an increase in temperature, one among several advantages of HT-PEMFCs (operating optimally between 160 to 180 °C) over low temperature PEM fuel cells (operating below 100 °C, typically around 80 °C). This is because increase in temperature favors $H_2$ adsorption over CO adsorption on Pt, due to the less exothermic nature of $H_2$ [11]. Moreover, increase in temperature promotes the electro-oxidation of the adsorbed CO into $CO_2$ [14,15], which is much less poisonous to the catalyst.

However, despite all the research recently done on the poisoning effects of CO and $CO_2$, studies on the possible poisoning effects of methanol vapor on HT-PEMFC are extremely scarce. The only knowledge about the effects of methanol on a PEM membrane comes from studies on direct methanol fuel cells (DMFCs), where crossover through the membrane with subsequent oxidation on the cathode side is the main mechanism by which performance is degraded [16]. Such an effect may be expected in PBI-based HT-PEMFCs as well, but this needs further investigation.

The present work addresses these issues and adds the effects of unconverted methanol-water vapor mixtures to the array of impurities to make the study of HT-PEMFC characterization more comprehensive. Degradation in this work is defined as the loss in fuel cell performance, both reversible and irreversible one. Degradation can be caused by catalytic degradation, surface adsorption of

impurities on the Pt surface or by means of Pt sintering, both manifested as losses of active electro-catalyst surface area (ECSA); or by membrane degradation, mainly phosphoric acid leaching and other unidentified mechanisms that can be caused by methanol-water vapor mixture.

## 2. Methodology

In the following the experimental setup, a brief summary of impedance spectroscopy applied to fuel cells, and the experimental procedures are described.

### *2.1. Experimental Set-up*

In Figure 1 the complete setup used to characterize the effects of reformate gas impurities in an HT-PEMFC is illustrated. It consists of a unit HT-PEM fuel cell assembly, mass flow controllers and a vapor delivery system. A typical $H_3PO_4$-doped PBI-based MEA for HT-PEMFC, BASF Celtec®- P2100 MEA, with an active surface area of 45 $cm^2$ was employed. The MEA was sandwiched between graphite composite flow plates of serpentine flow channels.

**Figure 1.** Experimental setup.

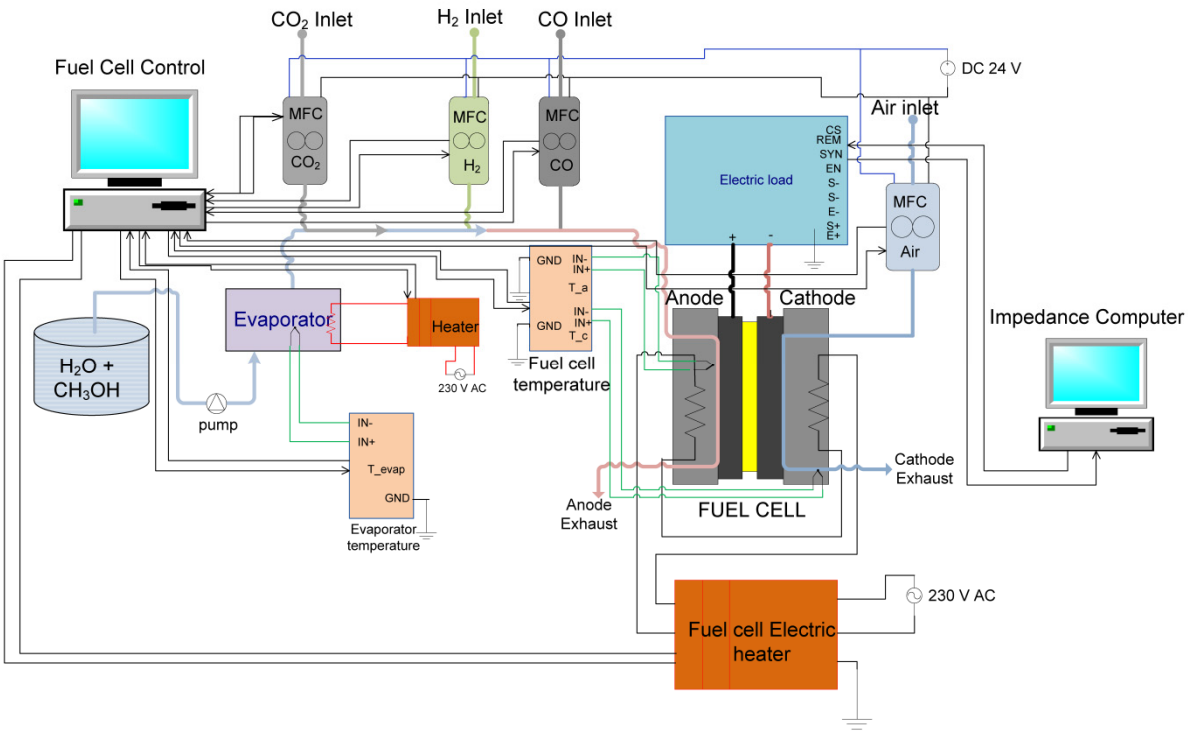


The mass flow controllers allow the entry into the fuel cell of the gaseous species involved, $H_2$ gas, $CO_2$, and CO on the anode side and air on the cathode side. It has to be said that the anode gases are not preheated before entering the anode. In reality in a system where reformate mixture is directly fed to the anode from a reformer, the gases are expected to be at the same temperature as the vapor constituents while entering the fuel cell. This is suspected to have negative effects, as CO adsorbs easier on the Pt-surface at lower temperatures. However, we expect this effect to be minor, since the fuel cell's operating temperature is kept constant by means of four electrical heaters, whose heating

power we believe is enough to minimize such undesired effects, and the gases would reach the cell temperature as soon as they are supplied.

A vapor delivery system was designed for the remaining constituents of the reformate gas, unconverted methanol vapor along with water vapor. This system, composed of a small high precision dosing pump and an electrically heated evaporator, delivers the vapor mixture in a controlled manner and at a fixed steam to carbon ratio. It was described in detail in our previous work [17].

The setup is entirely controlled and monitored by a control program in a LabView® environment, and impedance measurements were done using separate Gamry FC350 hardware and control software. Apart from the vapor delivery system, the setup is identical to the one described in [9].

### *2.2. Impedance Spectroscopy*

Impedance spectroscopy, also known as electrochemical impedance spectroscopy (EIS) or AC impedance, is a technique of characterization of electrochemical devices. It is done by measuring the electrical response of a material to small induced signal perturbances. These are then analysed to obtain useful information about the behavior of the device under various conditions.

Impedance is a complex function that can be calculated by Equation (1), using the amplitudes of the current, the voltage and the phase shift:

$$Z = (V_0\, e^{j(\omega t-\varphi)})/(I_0\, e^{j(\omega t)}) = (V_0\, e^{-j\varphi})/I_0 = Z_0\,(\cos\varphi - j\,\sin\varphi) \quad (1)$$

In Equation (1), $Z$ [Ω] is the complex impedance response of the system, $V_0$ [V] and $I_0$ [A] are the voltage and current signal amplitudes respectively, $\omega$ [rad/s] is the signal frequency and $\varphi$ [rad] is the voltage phase shift. Impedance has a real part ($Z_0 \cos\varphi$) and imaginary part ($Z_0 j \sin\varphi$). The information is normally presented on a Nyquist curve with real part on the horizontal axis and the imaginary on the vertical axis.

EIS was recently used extensively for optimization, characterization and diagnostics of fuel cells [18–23]. The different processes that occur in a cell respond differently to perturbances over a broad range of frequencies. In fact, if a fuel cell is perturbed on a broad range of frequencies, at low frequency the effects on slower processes with longer time constant like diffusion will be registered. At higher frequency however, effects on charge transfer would be sensed as they are much faster and have a much shorter time constant. The technique is described in detail in [24,25] for general application and in [18] for PEM fuel cells in particular.

One of the main advantages of EIS is that it is not intrusive and can be performed *in-situ*. It is a detailed technique with which information about different processes in the electrochemical device can be obtained with only little perturbation and since the perturbances are very small compared to the measured DC voltage or current, changes within the cell are minimal [26]. In a PEM fuel cell an AC perturbance of ~5% of the measured DC value can be suitably used [27].

In order to translate impedance measurement into more comprehensible figures and extract meaningful information, the analysis of data is typically done by fitting the measured data to an equivalent circuit model (EC) or a model based on physical properties that can reasonably represent the fuel cell under investigation. For better insight into the correct use of equivalent circuit modeling the reader is referred to [18,24,25].

### *2.3. Experimental Procedure*

The fuel cell was allowed to break-in, at 0.2 A/cm$^2$ (9 A), 160 °C for 100 hours, during which the stoichiometric ratios of hydrogen, $\lambda_{H2}$ and air, $\lambda_{Air}$ were kept constant at 2.5 and 3.5, respectively. A multilevel factorial design of experiments was chosen for thorough investigation of the effects of the different factors and their interdependence. Four factors, namely current density, concentration of methanol-water vapor mixture, CO concentration and $CO_2$ concentration were varied. The different factors and how they were varied in increasing levels is summarized in Table 1.

**Table 1.** The different factors and their levels used for the factorial design of experiments.

| **Factors** | **Levels** | | |
|---|---|---|---|
| Current Density [A/cm$^2$] | 0.22 | 0.33 | 0.44 |
| CO [% by volume] | 0 | 1 | 2 |
| $CO_2$ [% by volume] | 0 | 20 | |
| $CH_3OH$-$H_2O$ (g) [% by volume] | 0 | 5 | 10 |

Temperature was kept constant at 160 °C throughout the duration of the experiments. The runs were not randomized in order to avoid too much disruption of the steady-state operation, which would lead to longer waiting times between successive runs and perhaps to a premature failure of the fuel cell. Therefore, according to experience, factors that affect the equilibrium state the least were allowed to vary the most and the degree of contamination was made to increase progressively in time. This way a maximum number of allowable runs were achieved. At current density of 0.44 A/cm$^2$, measurements were limited to 5% methanol-water vapour mixture and 1% CO to avoid instability. Instability of the steady state equilibrium is observed in [28] at high CO concentrations.

In the process, the fuel cell continued to degrade, which inevitably changes the starting points for the different measurements at the different feed gas compositions and operation conditions. To avoid this, tests on as many identical unit cell test stations as the number of test points in a controlled environment would be required at prohibitive costs. In this work, the focus is on performing a preliminary qualitative study on the nature of the effects of the change in impurities concentration and not the magnitudes of the effects. Therefore, an accelerated approach is used to obtain a general understanding of the effects of all the impurities in a methanol reformate gas and the interactions among them. To achieve an accelerated degradation, all the reformate impurities were considered as stressors and varied during tests. As can be seen in Table 1, CO concentrations were tested up to 2%, $CO_2$ was tested up to 20% and methanol-water vapour mixture was tested up to 10% by volume of the anode feed composition.

Methanol steam reforming over $CuO/ZnO/Al_2O_3$ catalyst takes place according to three reactions [29], one of which is the desired reforming reaction [Equation (2)] and the other two are undesired; methanol decomposition [Equation (3)] and a reverse water gas shift reaction (RWGS) [Equation (4)]. The latter two need to be limited as they produce CO, which is the most poisonous among the constituents of a reformate gas. Considering the overall reaction [Equation (2)], which is the algebraic sum of the other two, the products of a complete reforming process are $CO_2$ and $H_2$ with a trace of CO, whose amount depends on the operating temperature and the molar ratio of $H_2O/CH_3OH$ (S/C). The three reactions are given below:

$$CH_3OH + H_2O \rightarrow CO_2 + 3H_2 \quad (2)$$

$$CH_3OH \leftrightarrow CO + 2H_2 \quad (3)$$

$$CO_2 + H_2 \leftrightarrow CO + H_2O \quad (4)$$

Usually an S/C ratio greater than 1 is used to minimize CO formation, leading to excess water vapour in the reformer output. Pan and Wang [30] found around 74.5% $H_2$ and 1% CO in dry gas composition with near 100% methanol conversion at S/C = 1.2. When lower reforming temperatures are desired for easier integration of fuel cells and reforming systems or for internal reforming, the methanol conversion could be significantly reduced and the reformate gas may contain unconverted methanol as seen in [31]. In the current work a rather high methanol content of 5%–10% by volume in feed gas is tested for an accelerated test and S/C ratio of 1 is considered as it gives the highest methanol concentration in water vapour in the reformate mixture.

For the same reason, due to the qualitative nature of the study, EIS alone is used in this work, which as mentioned above is a powerful tool for such kind of analysis. The use of polarization curves in conjunction with EIS is advisable when the performance of a fuel cell is to be analysed quantitatively, but this is not the case in the current work. A galvanostatic EIS is used, in which a perturbing AC current sinusoidal is applied and the voltage response is registered. For this, an AC sinusoidal of 0.5 A was applied, which is equal to 5% of the lowest current value (10 A) tested. This allows linearity assumption to hold for all measurements. Impedance spectra were acquired at different fuel cell operating conditions, while $H_2$ gas and air stoichiometric ratios were kept constant at 1.5 and 4, respectively. Measurements were done in the frequency range between 10 kHz and 1 Hz, and 10 points per decade were recorded.

For analysis and interpretation of impedance data, an EC model shown in Figure 2 was chosen. It is composed of lumped resistance (R) in series with two circuits, each comprising a resistance and a constant phase element (CPE) in parallel to each other. Ohmic resistance ($R_{ohmic}$), which is represented by the high frequency intercept on the horizontal axis, corresponds to the ohmic losses of the fuel cell, which are mainly due to the electrolyte resistance and contact resistances between interfaces. The other two resistances, high frequency resistance ($R_{hf}$) and intermediate-low frequency resistances ($R_{if}$) that form two arcs when put in parallel with the respective CPEs, are charge transfer resistances between electrode and electrolyte interfaces for high frequency range (10 kHz to ~125 Hz) and intermediate-low frequency range (~125 Hz to 1 Hz), respectively, and are sometimes controversially split between anode and cathode contributions.

**Figure 2.** Equivalent circuit with constant phase elements (CPE) used in this work.

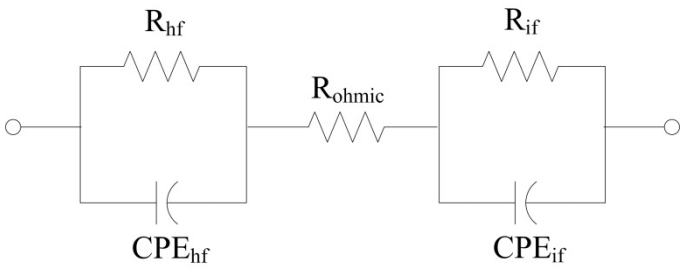

Constant phase elements are used instead of double layer capacitances to achieve better fits, and their exponential coefficients, α were kept constant at 0.75 for all the fits. Only resistances are allowed to change in the fitting software, ZView™ (Scribner Associates, Inc., Southern Pines, NC, USA). The software employs complex non-linear-least-square (CNLS) method for fitting and error estimation. For a better understanding of CNLS one can refer to [32]. The quality of the fit between the measured impedance data and the equivalent circuit model of choice is shown in Figure 3.

**Figure 3.** Fitting between measured impedance data and the chosen equivalent circuit model.

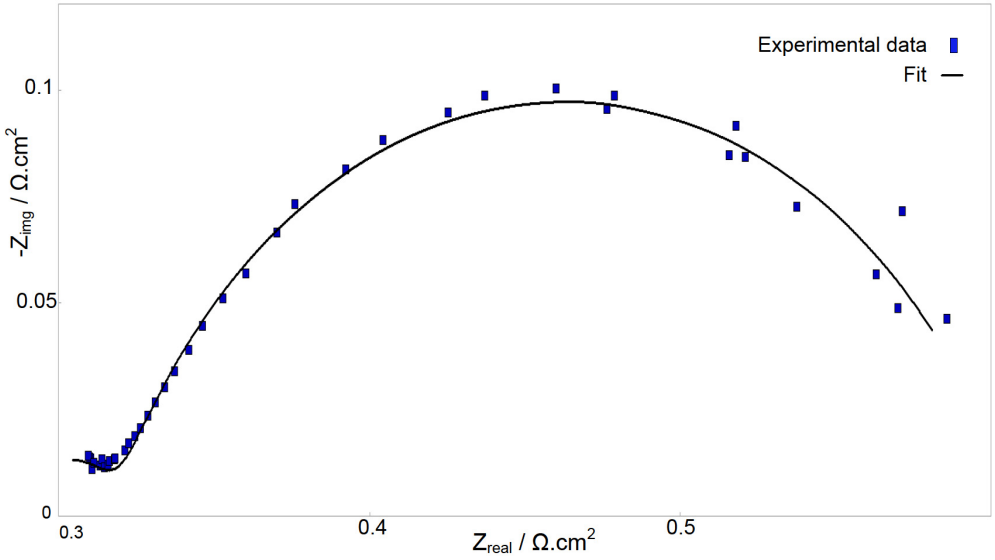


## 3. Results and Discussion

The results are divided into two subsections. In the first subsection, a general analysis on the mean values of the fitted data is presented, in which the interdependence among factors is also investigated. Then, analysis was made on fitted resistance values according to the progression in which tests were conducted. To assist in the analysis histograms were used to illustrate the trends of resistances for the different frequency ranges.

### *3.1. Analysis of Factors Interdependency*

First, the main effects of the various factors were analysed based on mean values of the fitted resistances, then interactions among factors were assessed. Figure 4 illustrates the main effects of methanol-water vapor mixture, CO, $CO_2$ and current density for the different regions of the frequency sweep.

From a main effects point of view, the results confirm that CO has the most severe poisoning effects of all the impurities in the whole range of frequency sweep. For $R_{hf}$ and $R_{if}$, this is in agreement with the existing notion that CO adsorbs on the Pt-surface and takes up active catalyst area. While there is not a clear explanation why the same effects are observed for $R_{ohmic}$, similar results are observed in [9], where the high frequency intercept that represents $R_{ohmic}$ moves to the right when CO is added.

**Figure 4.** Main effects of each factor at 160 °C. (**a**) Ohmic resistance; (**b**) High frequency resistance; (**c**) Intermediate -low frequency resistance.

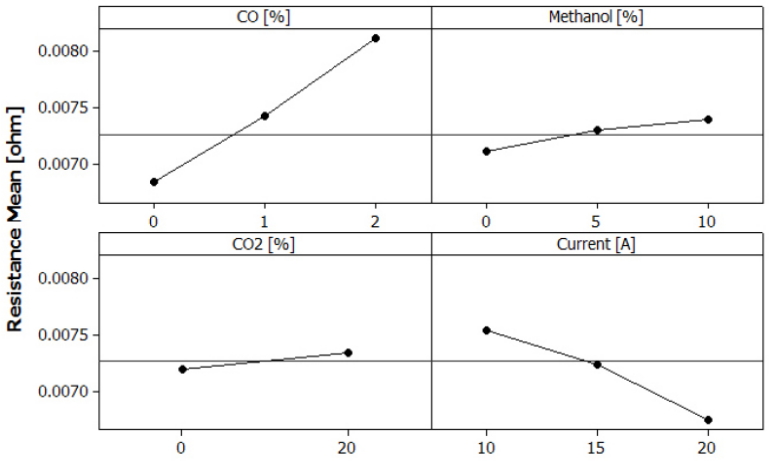


(**a**)

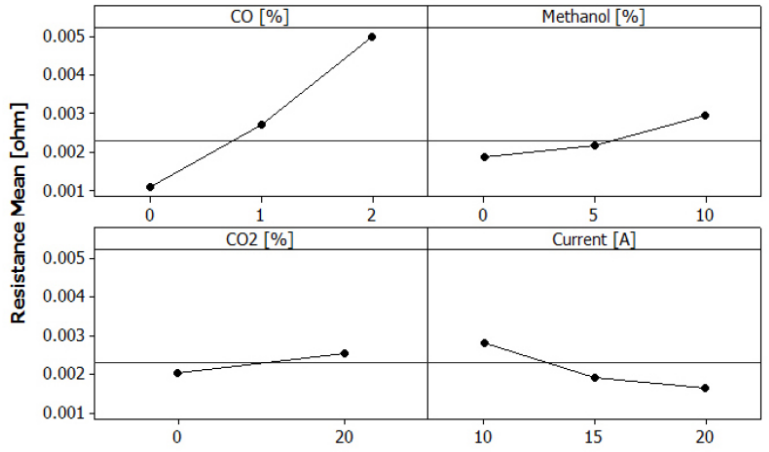


(**b**)

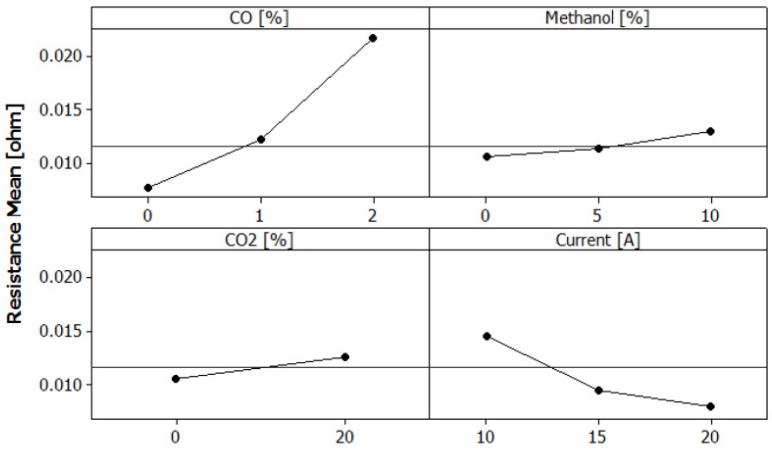


(**c**)

This could imply that CO somehow affects the PBI polymer membrane as well. In Figure 4, even though not significant, a small overall loss in fuel cell performance due to $CO_2$ is also seen. This could be either mere dilution of the reactants or some other $CO_2$ poisoning mechanisms are at play.

The interaction plots in Figure 5 show some interdependence between CO and $CO_2$, where the interaction seems not to exist for CO concentration below 1%, but is significant for CO concentration of 2%. Bhatia and Wang [33] found that the combined effects of trace quantities of CO and hydrogen dilution have an extremely detrimental effect on the performance of a LT-PEMFC. In our case the interaction is most significant for $R_{hf}$ and $R_{if}$, [Figure 5(b,c)], and negligible for $R_{ohmic}$, [Figure 5(a)]. Some interdependence among the effects of these two gases is also seen in [28]. In LT-PEMFCs the opposite is reported, where the losses due to $CO_2$ are the largest when the CO content is small [13,34]. Since the main $CO_2$ poisoning mechanism in LT-PEMFCs is through CO formation by RWGS, it could be that this effect decreases due to shift in equilibrium direction in the presence of CO or simply the effects of $CO_2$ are too small to be noticed compared to those of CO as LT-PEMFCs are very sensitive to CO. However, In HT-PEMFCs the worst effects of $CO_2$ are observed in the presence of CO [9], specifically 2% CO in our case. The main reason to this kind of interaction might be the same seen in [33], where the combined effects of CO and hydrogen dilution have detrimental effects on the performance of the fuel cell. This could be the result of reduced number of $H_2$ molecules per active catalyst area.

In addition, methanol-water vapor mixture, which is normally excluded from characterization tests, seems to have a poisoning effect at all frequency sweeps. The increase in vapor mixture concentration causes resistances to increase as in the case of CO and $CO_2$, with minimal increase, comparable to that of $CO_2$ observed for $R_{ohmic}$ and $R_{if}$. The increase is a little more pronounced for $R_{hf}$, especially when the concentration of methanol-water vapor mixture in anode feed gas is raised to 10% by volume. There is not much that can be found in the literature about the effects of methanol on HT-PEMFCs. It is reported that it is permeable, mainly via diffusion through $H_3PO_4$-doped PBI membranes [35,36], and that it electro-oxidises on the surface of Pt electrodes [37,38]. Moreover, methanol is known to undergo dehydrogenation on Pt surface according to the reaction below [37]:

$$CH_3OH + Pt \rightarrow Pt{-}CO + 4H^+ + 4e^- \quad (5)$$

As a consequence, the effects are interdependent with the effects of the other factors, especially with that of $CO_2$, as can be seen in Figure 5. As there are intermediate formations during methanol electro-oxidation on Pt-catalyst [39,40], the interaction could be with methanol itself or with the possible non-CO complex intermediates, such as formaldehyde and formic acid. The reason the interaction disappears in the case of 10% methanol could be, because the effects of $CO_2$ are overwhelmed by that of methanol at such high concentrations.

Current density also has its main effects, and little interdependence with some of the impurities as can be seen in Figures 4 and 5. Increase in current density causes decrease in resistance, with the effect being a little more pronounced in going from 0.22 A/cm$^2$ to 0.33 A/cm$^2$ than from 0.33 A/cm$^2$ to 0.44 A/cm$^2$. It does not show significant interdependence with the other factors as most of the trends are parallel to each other in the interaction plots in Figure 5. An exception is seen on its interaction with methanol-water vapor mixture in affecting $R_{ohmic}$, in the presence of 10% by volume of vapor mixture and in going from current densities of 0.33 A/cm$^2$ (15 A) to 0.44 A/cm$^2$ (20 A). Since no

interactions are seen at lower vapor mixture and lower current densities, and since the values of the factors were progressively increased, the effects of degradation cannot be overruled in the interdependence between these two factors.

Finally, it can be said that the collective effects of impurities on the performance of the fuel cell are greater than the arithmetic sum of effects in most cases. This is attributable to the possible reactions among impurities and their intermediates, and catalyst surface adsorptions of complex intermediate formations from the electro-oxidation of methanol on the catalyst surface.

**Figure 5.** Interaction of effects among the different factors at 160 °C. (**a**) Ohmic resistance; (**b**) High frequency resistance; (**c**) Intermediate -low frequency resistance.

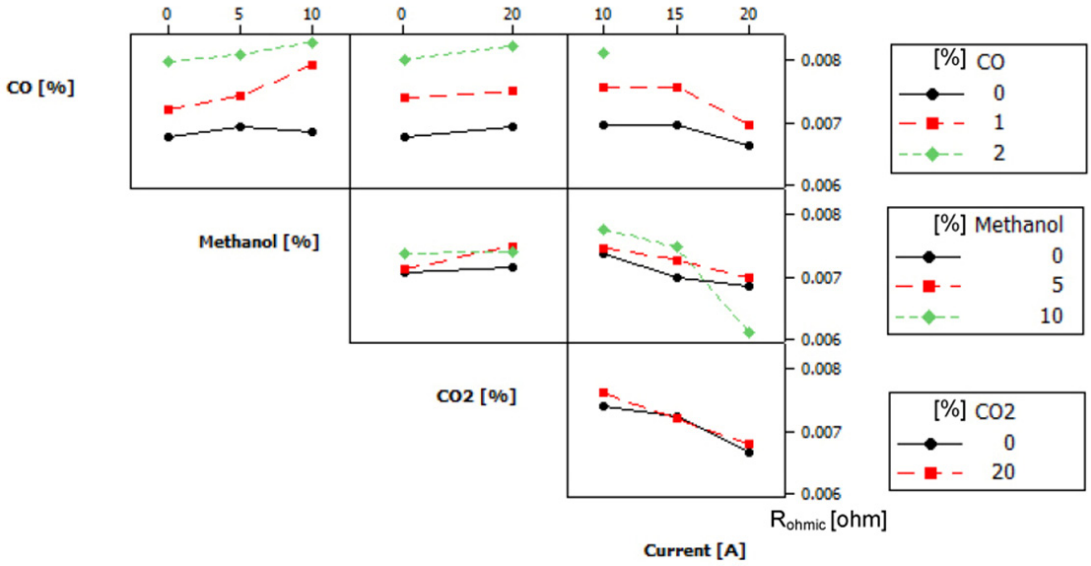


(**a**)

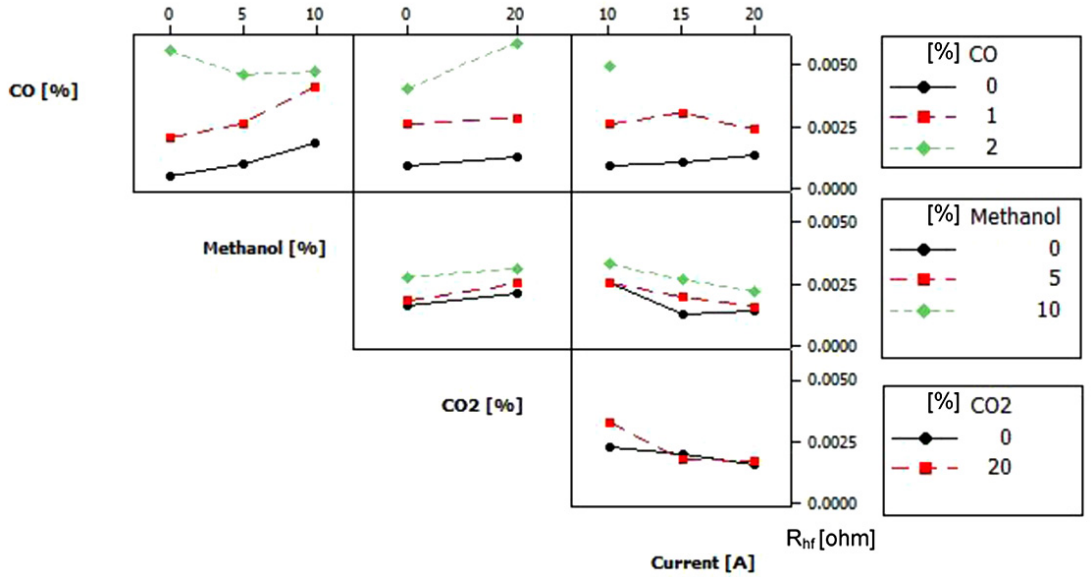


(**b**)

**Figure 5.** *Cont.*

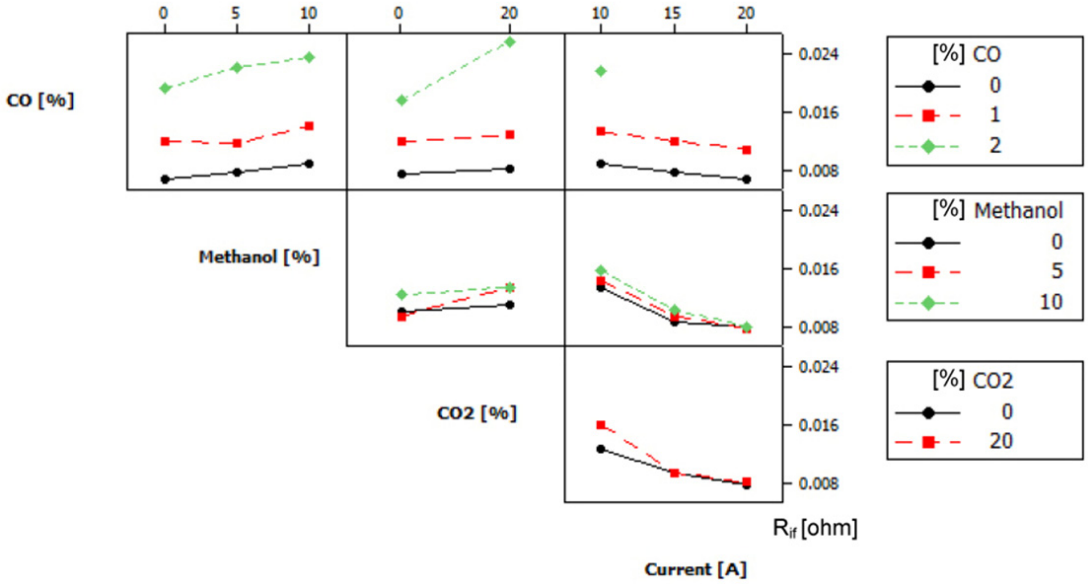


(**c**)

### *3.2. Progressive EIS Analysis*

#### 3.2.1. Current Density and $CO_2$

As already noted in other studies current density has the effect of increasing the activity in a fuel cell [19,27]. In Figure 6 it can be seen that as current density increases from 0.22 A/cm$^2$ (10 A) to 0.33 A/cm$^2$ (15 A) and then 0.44 A/cm$^2$ (20 A), the total impedance decreases and both the real and imaginary components of the impedance drop causing the semi-circles to shrink.

**Figure 6.** The effect of current density on a PBI-based HT-PEMFC operating at 160 °C both in the absence and in the presence of $CO_2$.

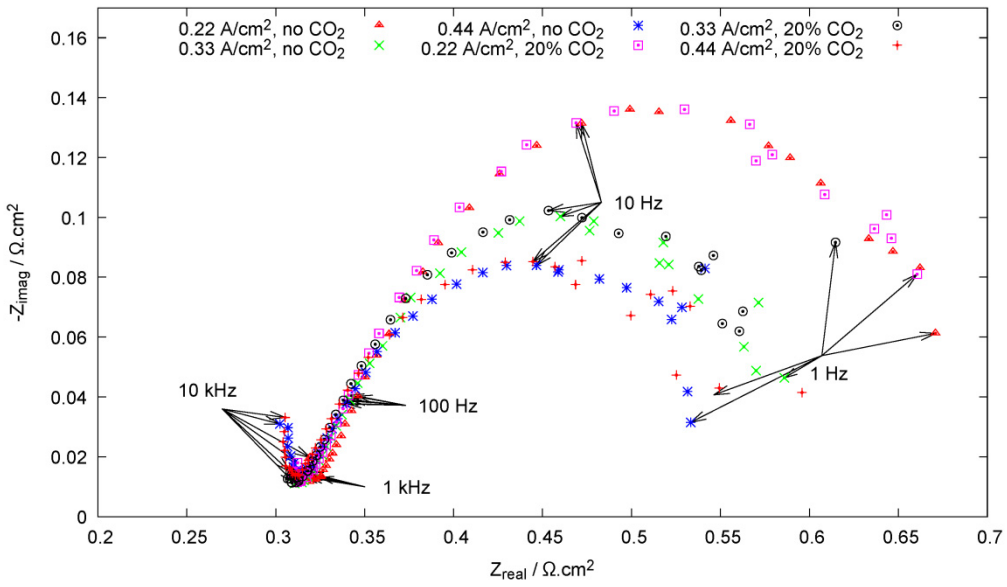

Figure 6 shows that the effects of current density remain almost the same, both in the case of pure $H_2$ gas and when 20% of the anode feed is $CO_2$. The only exception is seen at 0.22 A/cm$^2$, where the high frequency semi-circle is slightly shifted to the left in the presence of 20% $CO_2$, while the low frequency one remains unaltered. This shows that $CO_2$ alone does not have significant effect on the losses of a fuel cell, especially in this case, where the stoichiometric ratios and operating temperature are relatively high. It is reported that $CO_2$ is not completely inert and it loosely binds to Pt surface, and in the case of LT-PEMFC its poisoning effects increase with the increase in temperature as the kinetics of the RWGS increase to produce more CO [34]. This is not seen in HT-PEMFCs, possibly because the negative effects of the increase in RWGS kinetics is counteracted by the decrease in preferential CO adsorption and removal by electro-oxidation of adsorbed species at higher temperatures.

The histograms in Figure 7 and Figure 8 show that change in current density has little or no effects on $R_{ohmic}$ and $R_{hf}$. Similar negligible effect on $R_{hf}$ are also seen in [41]. Concerning $R_{ohmic}$ however, according to [19] there is increase in water production with increase in current density which may enhance the conductivity of the PBI-based membrane. This would imply a decrease in $R_{ohmic}$, which is not seen in this study, except for a very slight decrease in going from 0.22 A/cm$^2$ to 0.33 A/cm$^2$. Consequently, most of the effects of current density are displayed on $R_{if}$. This may be attributed to the increase in the flow of gases, as the hydrogen demand is calculated based on Faraday's law, in which more current corresponds to more hydrogen, and therefore more air.

**Figure 7.** The effect of methanol on a PBI-based HT-PEMFC operating at 160 °C with changing $CO_2$ content and current density. (**a**) Ohmic resistance; (**b**) High frequency resistance; (**c**) Intermediate -low frequency resistance.

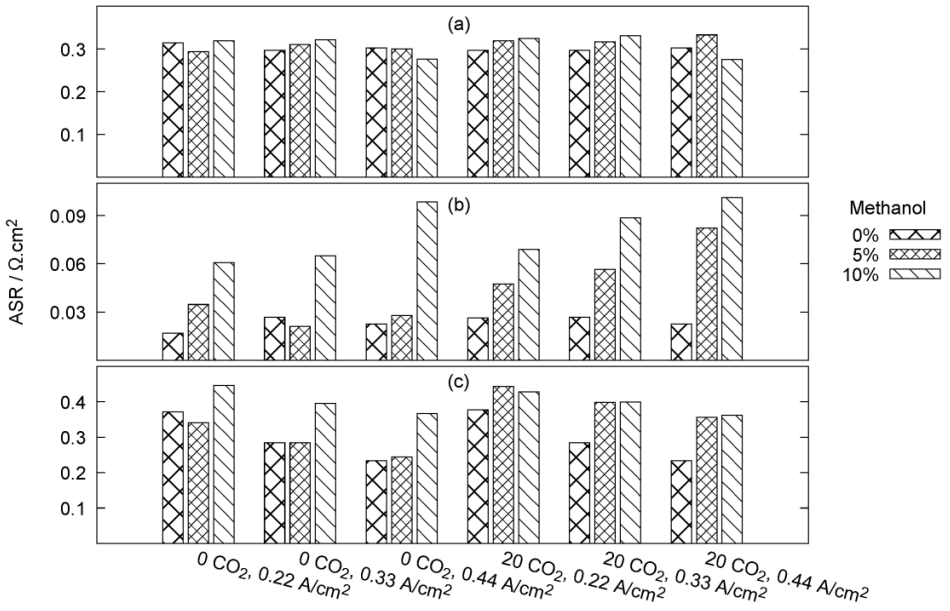


3.2.2. Current Density, $CO_2$ and Methanol

From the main effects in Figure 4, it is seen that increase in the concentration of methanol causes increase in resistance in all frequency ranges. If we look closely into the fitted results we can see the different trends for different operating conditions and obtain some insight on the electrochemistry behind the effects.

The fits as displayed in Figure 7 show the effect of methanol at 160 °C, where in Figure 7(a) methanol seems to increase the $R_{ohmic}$ for most of the operating conditions, with an exception at the highest current density, 0.44 A/cm$^2$. There is a slight decrease in the beginning as methanol is introduced. This could be because of the water vapor contained in the mixture, which is said to enhance the proton conduction of the PBI-based membranes [35]. However, this is seen only in the chronologically earlier measurements in the presence of methanol. Continued introduction of methanol on the other hand results in increased resistances, instead of enhancing the proton conductivity of the membrane.

High frequency resistance in Figure 7(b) is where the poisoning effects of methanol are most clearly visible. Here, resistances increase with increase in methanol vapor concentration for all operating conditions almost linearly. This could be because methanol undergoes some reactions or adsorbs on the anode side, where high frequency activities dominate. One of these reactions could be the dehydrogenation reaction mentioned above [Equation (5)] that gives rise to intermediate CO formation, which may adsorb on the Pt surface and reduce the electro-active catalyst area. The performance drop could also be due to methanol crossover with subsequent electro-oxidation on the surface of platinum, as in the case of DMFCs [16].

Intermediate-low frequency resistance in Figure 7(c) also has similar trend as that of $R_{hf}$ with increase in methanol content. However, it is interesting to notice that 5% methanol in the anode feed gas seems to have no effect in the absence of $CO_2$. This changes when $CO_2$ and methanol vapor are both present in the feed gas, where there is an evident increase in $R_{if}$ for 5% vapor mixture, but the effect of further increase in methanol content to 10% is negligible. The same phenomenon is also seen to a smaller extent for $R_{hf}$ in Figure 7(b). In short, it can be said that unlike in the case of pure hydrogen the effects of $CO_2$ are not insignificant when methanol-water vapor mixture is present in the feed gas.

**Figure 8.** The effect of methanol on a PBI-based HT-PEMFC operating at 160 °C and in the presence of 1% by volume of CO with changing $CO_2$ content and current density. (**a**) Ohmic resistance; (**b**) High frequency resistance; (**c**) Intermediate -low frequency resistance.

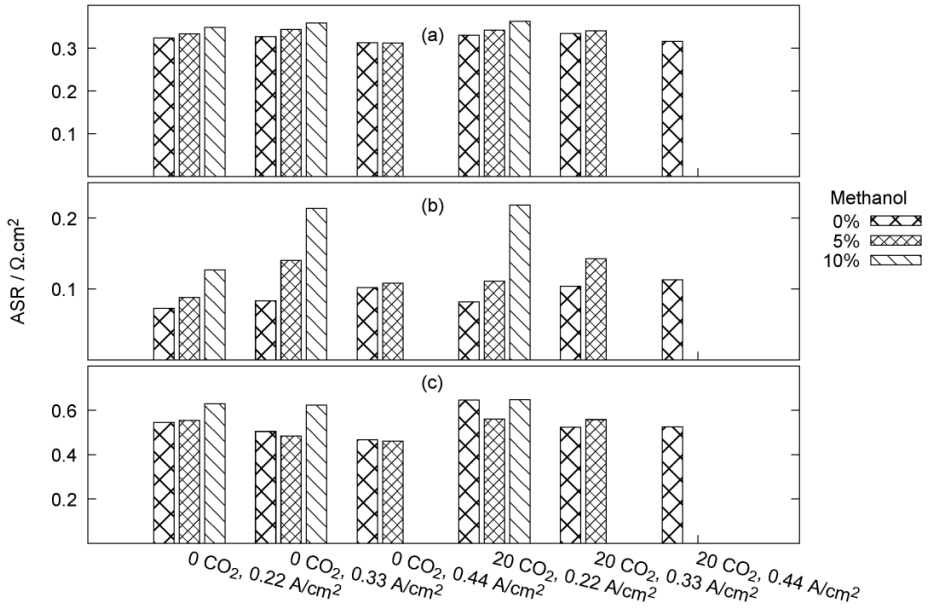

3.2.3. Current Density, $CO_2$, $CH_3OH$-$H_2O$ mixture, and CO

It can be seen in Figure 8 that the trends are similar to those without CO, where there is a general increase in resistances with increase in methanol content. This similar trend of the resistances with increase in methanol suggests the absence of interdependence between the effects of methanol and CO. This was apparent also from the interaction plots in Figure 5. However, the effects of both methanol and CO are dependent on the presence of $CO_2$, and since $CO_2$ content was varied equally in both cases, they each contribute to the sum of effects irrespective of the presence of the other.

A closer look at the data reveals that the addition of CO causes all resistances to sharply increase at all frequency sweeps compared to the former case, where only methanol-water vapor mixture and $CO_2$ were present. The increase is on average 8.6% for $R_{ohmic}$, 69% for $R_{hf}$ and 61% for $R_{if}$, confirming that the effects of CO are the most severe to HT-PEMFC, despite their relatively high tolerance to CO poisoning. In Figure 8(b) it can be seen that the effects are most clearly visible for $R_{hf}$, mainly because CO affects mainly Pt electro-catalyst [11]. It adsorbs on the active Pt sites of the electrodes, both anode and cathode (maybe through CO crossover) and inhibits the respective half-cell reactions, without affecting so much the proton conductivity of the electrolyte. The effect of CO poisoning on both anode and cathode is also reported in [15].

## 4. Conclusions

In an experimental characterization of a PBI-based HT-PEMFC, the effects of impurities from methanol steam reforming were investigated by means of EIS. It was found that all the impurities present in the reformate gas, that is CO, $CO_2$ and methanol-water vapor mixture, have poisoning effects on the fuel cell. This is true whether they are introduced individually or collectively as a mixed stream of gases and vapors. The results confirm that CO is the impurity with the most severe poisoning effects, while $CO_2$ has only minor effects, if present alone. High concentrations of methanol-water vapor mixture also degrade the performance of the fuel cell, and this should be considered when optimizing the operating parameters of reformate gas-fed HT-PEMFCs.

Factorial analysis shows some of the possible interdependence among the effects of the different impurities. The interaction is most important for CO and $CO_2$ at CO concentration of 2% by volume, suggesting that tolerance to CO of a PBI-based HT-PEMFC is reduced in the presence of $CO_2$. The study shows also a small interdependence among the effects of methanol-water vapor mixture and $CO_2$. Therefore, it can be said that the collective effects of impurities on the performance of the fuel cell are greater than the arithmetic sum of effects in most cases.

The interaction among effects obtained in this study gives an invaluable qualitative insight into the tolerable mixes of impurities for optimizing the operating parameters of an HT-PEMFC. This can be an input for tweaking the performance and selectivity of both the fuel cell and the methanol reforming processor. For a more complete picture of all factors, future work should include the history effect of time and its interdependence with the other factors.

## References


1. Ji, X.; Yan, L.; Zhu, S.; Zhang, L.; Lu, W. Methanol distribution and electroosmotic drag in hydrated poly(perfluorosulfonic) acid membrane. *J. Phys. Chem. B* **2008**, *112*, 15616–15627.
2. Ogden, J.M.; Steinbugler, M.M.; Kreutz, T.G. A comparison of hydrogen, methanol and gasoline as fuels for fuel cell vehicles: implications for vehicle design and infrastructure development. *J. Power Sources* **1999**, *79*,143–168.
3. Bromberg, L.; Cheng, W.K. *Methanol as an Alternative Transportation Fuel in the U.S.: Options for Sustainable and/or Energy-Secure Transportation*; Technical Report for Massachusetts Institute of Technology, Sloan Laboratories for Automotive and Aircraft Engines: Cambridge, MA, USA, November 2010.
4. Olah, G.A.; Goeppert, A.; Prakash, G.K. S. *Beyond Oil and Gas: The Methanol Economy*, 2nd ed.; Wiley-VCH: Weinheim, Germany, 2009.
5. Methanex Corporation®. *Technical Information and Safe Handling Guide for Methanol*; Vancouver, Canada, 2006.
6. Pan, C.; He, R.; Li, Q.; Jensen, J.O.; Bjerrum, N.J.; Hjulmand, H.A.; Jensen, A.B. Integration of high temperature PEM fuel cells with a methanol reformer. *J. Power Sources* **2005**, *145*, 392–398.
7. Ouzounidou, M.; Ipsakis, D.; Voutetakis, S.; Papadopoulou, S.; Seferlis, P. A Combined methanol autothermal steam reforming and PEM fuel cell pilot plant unit: Experimental and simulation studies. *Energy* **2009**, *34*, 1733–1743.
8. Bhatia, K.K. Study of Methanol Reforming Polymer Electrolyte Fuel Cell System. Ph.D. Thesis, College of Engineering, The Graduate School, The Pennsylvania State University, PA, USA, August 2004.
9. Andreasen, S.J.; Vang, J.R.; Kær, S.K. High temperature PEM fuel cell performance characterisation with CO and $CO_2$ using electrochemical impedance spectroscopy. *Int. J. Hydrog. Energy* **2011**, *3*, 9815–9830.
10. Du, B.; Pollard, R.; Elter, J.F.; Ramani, M. In *Polymer Electrolyte Fuel Cell Durability*; Buchi, F.N., Inaba, M., Schmidt, T.J., Eds.; Springer: New York, NY, USA, 2009; pp. 341–366.
11. Zhang, J.; Xie, Z.; Zhang, J.; Tang, Y.; Song, C.; Navessin, T.; Shi, Z.; Song, D.; Wang, H.; Wilkinson, D.P.; *et al*. High Temperature PEM Fuel Cells. *J. Power Sources* **2006**, *160*, 872–891.
12. Das, S.K.; Reis, A.; Berry, K. Experimental evaluation of CO poisoning on the performance of a high temperature proton exchange membrane fuel cell. *J. Power Sources* **2009**, *193*, 691–698.
13. Yan, W.M.; Chu, H.S.; Lu, M.X.; Weng, F.B.; Jung, G.B.; Lee, C.Y. Degradation of Proton Exchange Membrane Fuel Cells Due to CO and $CO_2$ Poisoning. *J. Power Sources* **2009**, *188*,141–147.
14. Bellows, R.; Marucchi-Soos, E.; Buckley, D. Analysis of reaction kinetics for carbon monoxide and carbon dioxide on polycrystalline platinum relative to fuel cell operation. *Ind. Eng. Chem. Res*. **1996**, *3*, 1235–1242.
15. Cheng, X.; Shi, Z.; Glass, N.; Zhang, L.; Zhang, J.; Song, D.; Liu, Z.S.; Wang, H.; Shen, J. A review of PEM hydrogen fuel cell contamination: Impacts, mechanisms, and mitigation. *J. Power Sources* **2007**, *165*, 739–756.

16. Du, C.; Zhao, T.; Yang, W. Effect of methanol crossover on the cathode behavior of a DMFC: A half-cell investigation. *Electrochim. Acta* **2007**, *52*, 5266–5271.
17. Araya, S.S.; Kær, S.K.; Andreasen, S.J. Vapor delivery systems for the study of the effects of reformate gas impurities in HT-PEM fuel cells. *J. Fuel Cell Sci. Technol.* **2012**, *9*, 015001–015006.
18. Yuan, X.Z.; Song, C.; Wang, H.; Zhang, J. *Electrochemical Impedance Spectroscopy in PEM Fuel Cells: Fundamentals and Applications*; Springer: London, UK, 2010; pp. 139–191.
19. Mamlouk, M.; Scott, K. Analysis of high temperature polymer electrolyte membrane fuel cell electrodes using electrochemical impedance spectroscopy. *Electrochim. Acta* **2011**, *56*, 5493–5512.
20. Zhang, J.; Zhang, L.; Bezerra, C.W.; Li, H.; Xia, Z.; Zhang, J.; Marques, A.L.; Marques, E.P. EIS assisted performance analysis of non-noble metal electro-catalyst (FeN/C)-based PEM fuel cells in the temperature range of 23–80 °C. *Electrochim. Acta* **2009**, *54*, 1737–1743.
21. Asghari, S.; Mokmeli, A.; Samavati, M. Study of PEM fuel cell performance by electrochemical impedance spectroscopy. *Int. J. Hydrog. Energy* **2010**, *35*, 9283–9290.
22. Fouquet, N.; Doulet, C.; Nouillant, C.; Tanguy, G.D.; Bouamama, B.O. Model based PEM fuel cell state-of-health monitoring via AC impedance measurements. *J. Power Sources* **2006**, *159*, 905–913.
23. Pattamarat, K.; Hunsom, M. Testing of PEM fuel cell performance by electrochemical impedance spectroscopy: Optimum condition for low relative humidification cathode. *Korean J. Chem. Eng.* **2008**, *25*, 245–252.
24. Barsoukov, E.; Macdonald, J.R. *Impedance Spectroscopy: Theory, Experiment, and Applications*, 2nd ed.; Wiley-Interscience: Hoboken, NJ, USA, 2005.
25. Orazem, M.E.; Tribollet, B. *Electrochemical Impedance Spectroscopy*; John Wiley & Sons: Hoboken, NJ, USA, 2008.
26. Monk, P. *Fundamentals of Electroanalytical Chemistry, Analytical Techniques in the Sciences*; John Wiley & Sons: Chichester, West Sussex, England, 2007.
27. Yuan, X.; Wang, H.; Sun, J.C.; Zhang, J. AC impedance technique in PEM fuel cell diagnosis–A review. *Int. J. Hydrog. Energy* **2007**, *32*, 4365–4380.
28. Andreasen, S.J.; Mosbæk, R.; Vang, J.R.; Kær, S.K.; Araya, S.S. EIS characterization of the poisoning effects of CO and $CO_2$ on a PBI based HT-PEM fuel cell. In *Proceeding of the 8th International Conference on Fuel Cell Science, Engineering and Technology*, New York, NY, USA, 14–16 June 2010; pp. 27–36.
29. Peppley, B.A.; Amphlett, J.C.; Kearns, L.M.; Mann, R.F. Methanol-Steam reforming on $Cu/ZnO/Al_2O_3$. Part 1: the Reaction Network. *Appl. Catal.* **1999**, *179*, 21–29.
30. Pan, L.; Wang, S. Modeling of a compact plate-fin reformer for methanol steam reforming in fuel cell systems. *Chem. Eng. J.* **2005**, *108*, 51–58.
31. Agrell, J.; Birgersson, H.; Boutonnet, M. Steam reforming of methanol over a $Cu/ZnO/Al_2O_3$ catalyst: A kinetic analysis and strategies for suppression of CO formation. *J. Power Sources* **2002**, *106*, 249–257.
32. Tsai, Y.T.; Whitmore, D. Nonlinear least-squares analyses of complex impedance and admittance data for solid electrolytes. *Solid State Ion.* **1982**, *7*, 129–139.

33. Bhatia, K.K.; Wang, C.Y. Transient carbon monoxide poisoning of a polymer electrolyte fuel cell operating on diluted hydrogen feed. *Electrochim. Acta* **2004**, *49*, 2333–2341.
34. De Bruijn, F.A.; Papageorgopoulos, D.C.; Sitters, E.F.; Janssen, G.J.M. The Influence of Carbon Dioxide on PEM Fuel Cell Anodes. *J. Power Sources* **2002,** *110*, 117–124.
35. Daletou, M.K.; Kallitsis, J.K.; Voyiatzis, G.; Neophytides, S.G. The interaction of water vapors with $H_3PO_4$ imbibed electrolyte based on PBI/polysulfone copolymer blends. *J. Memb. Sci.* **2009**, *326*, 76–83.
36. Li, Q.; Jensen, J.O.; Savinell, R.F.; Bjerrum, N.J. High temperature proton exchange membranes based on polybenzimidazoles for fuel cells. *Prog. Polym. Sci.* **2009**, *34*, 449–477.
37. Sriramulu, S.; Jarvi, T.; Stuve, E. Reaction Mechanism and Dynamics of Methanol Electrooxidation on Platinum (111). *J. Electroanal. Chem.* **1999**, *467*, 132–142.
38. Spendelow, J.; Babu, P.; Wieckowski, A. Electrocatalytic oxidation of carbon monoxide and methanol on platinum surfaces decorated with ruthenium. *Curr. Opin. Solid State Mater. Sci.* **2005**, *9*, 37–48.
39. Cao, D.; Lu, G.Q.; Wieckowski, A; Wasileski, S.A.; Neurock, M. Mechanisms of methanol decomposition on platinum: A combined experimental and *ab initio* approach. *J. Phys. Chem. B* **2005**, *109*, 11622–11633.
40. Iwasita, T. Electrocatalysis of methanol oxidation. *Electrochim Acta* **2002**, *47*, 3663–3674.
41. Makharia, R.; Mathias, M.F.; Baker, D.R. Measurement of catalyst layer electrolyte resistance in PEFCs using electrochemical impedance spectroscopy. *J. Electrochem. Soc.* **2005**, *152*, 970–977.